

DIGITAL ACCESS TO SCHOLARSHIP AT HARVARD
DASH.HARVARD.EDU

HARVARD LIBRARY


Detection of an Extrasolar Planet Atmosphere

Citation

Charbonneau, David, Timothy M. Brown, Robert W. Noyes, and Ronald L. Gilliland. 2002. "Detection of an Extrasolar Planet Atmosphere." The Astrophysical Journal 568 (1): 377–84. https://doi.org/10.1086/338770.

Published version

https://doi.org/10.1086/338770

Link

http://nrs.harvard.edu/urn-3:HUL.InstRepos:41397433

Terms of use

This article was downloaded from Harvard University's DASH repository, and is made available under the terms and conditions applicable to Other Posted Material (LAA), as set forth at https://harvardwiki.atlassian.net/wiki/external/NGY5NDE4ZjgzNTc5NDQzMGIzZWZhMGFlOWI2M2EwYTg

Accessibility

https://accessibility.huit.harvard.edu/digital-accessibility-policy

Share Your Story

The Harvard community has made this article openly available.
Please share how this access benefits you. Submit a story

The Astrophysical Journal, 568:377–384, 2002 March 20
© 2002. The American Astronomical Society. All rights reserved. Printed in U.S.A.

DETECTION OF AN EXTRASOLAR PLANET ATMOSPHERE[1]

David Charbonneau,[2,3] Timothy M. Brown,[4] Robert W. Noyes,[3] and Ronald L. Gilliland[5]
Received 2001 October 25; accepted 2001 November 19

ABSTRACT

We report high-precision spectrophotometric observations of four planetary transits of HD 209458, in the region of the sodium resonance doublet at 589.3 nm. We find that the photometric dimming during transit in a bandpass centered on the sodium feature is deeper by $(2.32 \pm 0.57) \times 10^{-4}$ relative to simultaneous observations of the transit in adjacent bands. We interpret this additional dimming as absorption from sodium in the planetary atmosphere, as recently predicted from several theoretical modeling efforts. Our model for a cloudless planetary atmosphere with a solar abundance of sodium in atomic form predicts more sodium absorption than we observe. There are several possibilities that may account for this reduced amplitude, including reaction of atomic sodium into molecular gases and/or condensates, photoionization of sodium by the stellar flux, a low primordial abundance of sodium, and the presence of clouds high in the atmosphere.

Subject headings: binaries: eclipsing — planetary systems — stars: atmospheres — stars: individual (HD 209458) — techniques: photometric

1. INTRODUCTION

Since the discovery of planetary transits in the light curve of HD 209458 (Charbonneau et al. 2000; Henry et al. 2000; Mazeh et al. 2000), this star has been the subject of intensive study. Multicolor observations (Jha et al. 2000; Deeg, Garrido, & Claret 2001) have confirmed the expected color dependence of the light curve due to the stellar limb darkening. Radial velocity monitoring during transit (Queloz et al. 2000a; Bundy & Marcy 2000) has yielded variations in excess of the orbital motion, as a result of the occultation of the rotating stellar limb by the planet. Very high precision photometry (Brown et al. 2001, hereafter B01) has permitted an improved estimate of the planetary and stellar radii, orbital inclination, and stellar limb darkening, as well as a search for planetary satellites and circumplanetary rings.

Transiting extrasolar planets present a unique opportunity for us to learn about the atmospheres of the objects. Wavelength-dependent variations in the height at which the planet becomes opaque to tangential rays will result in wavelength-dependent changes in the ratio of spectra taken in and out of transit. Several groups (Seager & Sasselov 2000; Brown 2001; Hubbard et al. 2001) have pursued theoretical explorations of this effect for a variety of model planetary atmospheres. These studies have demonstrated that clouds, varying temperature structure and chemical composition, and even atmospheric winds all produce variations that would be observed, should the requisite precision be achieved. Based on these calculations, the expected variations could be as large as 0.1% relative to the stellar continuum.

A previous search by Bundy & Marcy (2000) for variations between spectra of HD 209458 observed in and out of transit (using extant spectra gathered for radial velocity measurements) was sensitive to features with a relative intensity greater than 1%–2% of the stellar continuum. Moutou et al. (2001) conducted a similar study and achieved a detection threshold of 1%. Although the precision achieved by both these studies was insufficient to address any reasonable model of the planetary atmosphere, Moutou et al. (2001) placed limits on the models of the planetary exosphere. Searches for absorption due to a planetary exosphere have also been conducted for 51 Peg during the times of inferior conjunction (Coustenis et al. 1998; Rauer et al. 2000).

2. OBSERVATIONS AND DATA ANALYSIS

We obtained 684 spectra[6] of HD 209458 with the *HST* STIS spectrograph, spanning the times of four planetary transits, on UT 2000 April 25, April 28–29, May 5–6, and May 12–13. The primary science goal of this project was to improve the estimate of the planetary and stellar radii, orbital inclination, and stellar limb darkening, as well as to conduct a search for planetary satellites and circumplanetary rings; we presented these results in B01. In selecting the wavelength range for these observations, the desire to maximize the number of detected photons led us to consider regions near 600 nm, where the combination of the instrumental sensitivity and the stellar flux would be optimized.

The secondary science goal was to pursue the prediction by Seager & Sasselov (2000) (and, later, Brown 2001; Hubbard et al. 2001) of a strong spectroscopic feature at 589.3 nm due to absorption from sodium in the planetary atmosphere. Thus, we chose to observe the wavelength region $581.3 \text{ nm} \leq \lambda \leq 638.2$ nm, with a medium resolution of

[1] Based on observations with the NASA/ESA *Hubble Space Telescope* (*HST*), obtained at the Space Telescope Science Institute, which is operated by the Association of Universities for Research in Astronomy, Inc. under NASA contract NAS 5-26555.

[2] Department of Astronomy, California Institute of Technology, 105-24, 1200 East California Boulevard, Pasadena, CA 91125; dc@astro.caltech.edu.

[3] Harvard-Smithsonian Center for Astrophysics, 60 Garden Street, Cambridge, MA 02138; rnoyes@cfa.harvard.edu.

[4] High Altitude Observatory/National Center for Atmospheric Research, 3450 Mitchell Lane, Boulder, CO 80307; timbrown@hao.ucar.edu. The National Center for Atmospheric Research is sponsored by the National Science Foundation.

[5] Space Telescope Science Institute, 3700 San Martin Drive, Baltimore, MD 21218; gillil@stsci.edu.

[6] These data are publicly available at http://archive.stsci.edu.

TABLE 1
WAVELENGTH BANDS

	BLUE		CENTER		RED	
WIDTH	Identifier	Wavelength (nm)	Identifier	Wavelength (nm)	Identifier	Wavelength (nm)
Narrow	n_b	581.8–588.7	n_c	588.7–589.9	n_r	589.9–596.8
Medium	m_b	581.8–587.4	m_c	587.4–591.2	m_r	591.2–596.8
Wide	w_b	581.8–584.3	w_c	584.3–594.3	w_r	594.3–596.8

$R = \lambda/\Delta\lambda = 5540$, corresponding to a resolution element of 0.11 nm.

The details of the data acquisition and analysis are presented in B01, and we refer the reader to that publication. In summary, the data reduction consisted of (1) recalibrating the two-dimensional CCD images, (2) removing cosmic-ray events, (3) extracting one-dimensional spectra, (4) summing the detected counts over wavelength to yield a photometric index, and (5) correcting the resulting photometric time series for variations that depend on the phase of the *HST* orbit and for variations between visits. The only difference in these procedures between B01 and the current work is in step 4. Previously, we summed the spectra either (*a*) over the entire available wavelength range or (*b*) over the blue and red halves of the available range. In the present paper, we restrict greatly the wavelength span over which we perform the integration.

As described in B01, observations of the first transit (UT 2000 April 25) were partly compromised by a database error in the location of the position of the spectrum on the detector. The result was that the spectrum was not entirely contained within the CCD subarray. In the subsequent data analysis, we ignored these data. Furthermore, as described in B01, the first orbit (of five) for each visit shows photometric variability in excess of that achieved for the remaining orbits. These variations are presumably due to the spacecraft; we omit these data as well. This leaves 417 spectra of the 684 acquired.

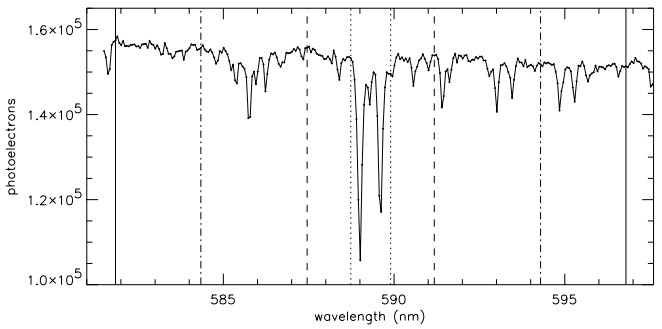


FIG. 1.—Portion of an STIS spectrum of HD 209458, centered on the Na D lines. The vertical axis is the number of detected photoelectrons per wavelength pixel after integrating over 17 pixels in cross-dispersion. The vertical lines indicate the bandpasses over which we integrate the spectrum to produce the photometric time series. The band n_c is the set of pixels between the two dotted lines; m_c is the set between the dashed lines; w_c is the set between the dot-dashed lines. The corresponding blue bands (n_b, m_b, and w_b) are the sets of pixels between the left solid line and the left boundary of the center band. Similarly, the corresponding red bands (n_r, m_r, and w_r) are the sets of pixels between the right edge of the center band and the right solid line.

Because we do not know the precise width of the feature we seek, we select three bands of varying width, each centered on the sodium feature. We refer to these bands as "narrow" (*n*), "medium" (*m*), and "wide" (*w*). The *n* band is the smallest wavelength range that still encompasses the stellar sodium lines; the *w* band is the widest wavelength range that permits an adjacent calibrating band to the blue. The *m* band is roughly intermediate (by ratio) between these two extremes; it is $\sim\frac{1}{3}$ the range of the *w* band, and $\sim$3 times the range of the *n* band. We further define, for each of these, a "blue" (*b*) and a "red" (*r*) band, which bracket the "center" (*c*) band. The names and ranges of these nine bands are given in Table 1 and displayed in Figure 1. For each of these nine bands, we produce a photometric time series by the procedure described above. The photometric index at a time *t* is then identified by a letter indicating the width and a subscript indicating the position [e.g., "$w_r(t)$" indicates the photometric index in the wide band, red side, at time *t*]. Each of these is a normalized time series, with a value of unity when averaged over the out-of-transit observations; the minimum values near the transit centers are approximately 0.984.

We denote the time of the center of the photometric transit by T_c. In what follows, we consider the in-transit observations, (i.e., those that occur between second and third contacts, $|t - T_c| < 66.111$ minutes), which we denote by $t_{\rm in}$, and the out-of-transit observations (those that occur before first contact, or after fourth contact, $|t - T_c| > 92.125$ minutes), which we denote by $t_{\rm out}$. There are 171 in-transit observations and 207 out-of-transit observations. We ignore the small fraction (7%) of observations that occur during ingress or egress.

2.1. *Stellar Limb Darkening*

One potential source of color-dependent variation in the transit shape is stellar limb darkening (see Fig. 6 of B01; also Jha et al. 2000; Deeg et al. 2001). In order to investigate this possibility, we produce (for each width) the difference of the red and blue bands:

$$\begin{aligned} n_d(t) &= n_b(t) - n_r(t) \\ m_d(t) &= m_b(t) - m_r(t) \\ w_d(t) &= w_b(t) - w_r(t)\ . \end{aligned} \tag{1}$$

The observed standard deviations in these time series (measured over the out-of-transit observations) are $\sigma[n_d(t_{\rm out})] = 3.3 \times 10^{-4}$, $\sigma[m_d(t_{\rm out})] = 3.6 \times 10^{-4}$, and $\sigma[w_d(t_{\rm out})] = 5.4 \times 10^{-4}$. These values match the predictions based on photon noise.

In order to check for changes in the transit depth due to stellar limb darkening, we then calculate, for each of the

time series above, the difference between the mean of the relative flux for in-transit observations and that for out-of-transit observations:

$$\Delta n_d = \overline{n_d(t_{\rm in})} - \overline{n_d(t_{\rm out})} = (-2.0 \pm 2.5) \times 10^{-5}$$
$$\Delta m_d = \overline{m_d(t_{\rm in})} - \overline{m_d(t_{\rm out})} = (+0.1 \pm 2.7) \times 10^{-5}$$
$$\Delta w_d = \overline{w_d(t_{\rm in})} - \overline{w_d(t_{\rm out})} = (-3.1 \pm 4.1) \times 10^{-5} . \quad (2)$$

Overbars indicate averages over time, and each quoted error is the estimated standard deviation of the mean. All of these values are consistent with no variation. Thus, we have no evidence of color-dependent limb darkening between these bands, which span about 15 nm.

We compared these results with predictions based on a theoretical model of the stellar surface brightness. The model was produced by R. Kurucz (2000, private communication). We denote it by $S(\lambda, \mu)$, where μ is the cosine of the angle between the line of sight and the normal to the local stellar surface. The stellar parameters were taken to be the best-fit values as found by Mazeh et al. (2000): $T_{\rm eff} = 6000$ K, $\log g = 4.25$, and [Fe/H] = 0.00. The model is evaluated at a spectral resolution of $R = 2{,}000{,}000$ (greatly in excess of the STIS resolution, $R = 5540$), and at 17 values of $\mu \in [0, 1]$.

The stellar model allows us to produce a theoretical transit curve, over a chosen bandpass, that includes the effects of stellar limb darkening. We do not force the limb darkening to fit a parameterized model. Rather, we interpolate between the values of μ on which the model of $S(\lambda, \mu)$ is initially calculated. For each λ, we produce the theoretical transit curve $T(\lambda, t)$ for all t at which we have data. The curve is calculated by integrating over the unocculted portion of the stellar disk, as described in Charbonneau et al. (2000) and Sackett (1999). We assume the best-fit values from B01 for the stellar radius ($R_s = 1.146\ R_\odot$), planetary radius ($R_p = 1.347\ R_{\rm Jup}$, where $R_{\rm Jup} = 71{,}492$ km is the equatorial radius of Jupiter at a pressure of 1 bar; Cox 2000), orbital period ($P = 3.52474$ days), orbital inclination ($i = 86.^\circ6$), and semimajor axis ($a = 0.0468$ AU), assuming a value for the stellar mass of $M_s = 1.1\ M_\odot$ (Mazeh et al. 2000).

We note that the STIS data have an effective continuum that is tilted relative to the theoretical values, because of the wavelength-dependent sensitivity of the instrument. We wish to emulate the data, where each λ is weighted by the observed number of photons. To do so, we fit a low-order polynomial (in λ) to the model disk-integrated spectrum and a second low-order polynomial to the STIS data. We subsequently divide the calculated $T(\lambda, t)$ for each t by the ratio of these polynomials.

Next, we integrate $T(\lambda, t)$ in λ over each of the bandpasses in Table 1. We subsequently difference the model light curve, as calculated for the blue and red bands (emulating what we did with the data in eq. [1]), and then evaluate the mean of the difference (as in eq. [2]):

$$\Delta n_d({\rm theory}) = -0.44 \times 10^{-5}$$
$$\Delta m_d({\rm theory}) = -0.58 \times 10^{-5}$$
$$\Delta w_d({\rm theory}) = -0.85 \times 10^{-5} . \quad (3)$$

These results can be compared directly with equation (2). Each of these is much smaller than the observational precision we achieved and thus consistent with our observational result of no significant offset.

Furthermore, the results stated in equation (2) demonstrate that the data remain photon noise–limited at these high levels of precision. We have taken the mean of two large groups of data (roughly 200 observations apiece) and found that the difference is consistent with photon noise–limited photometry, with a typical precision of 3×10^{-5}.

2.2. *The Sodium Band*

In order to search for variations in the sodium band relative to the adjacent bands, we produce (for each width) the mean light curve of the blue and red bands and difference this from the light curve for the center band:

$$n_{\rm Na}(t) = n_c(t) - [n_b(t) + n_r(t)]/2$$
$$m_{\rm Na}(t) = m_c(t) - [m_b(t) + m_r(t)]/2$$
$$w_{\rm Na}(t) = w_c(t) - [w_b(t) + w_r(t)]/2 . \quad (4)$$

This linear combination removes the variations due to the color dependence of the limb darkening of the stellar continuum. As we found above (§ 2.1), this effect is very small (eq. [3]). We consider the effect of the deviations in the limb darkening that occur in the cores of stellar absorption features in § 4.1 and show that this effect is also negligible. The three time series in equation (4) are plotted as a function of absolute value of the time from the center of transit in Figure 2. The observed standard deviations in these time series over the out-of-transit observations are $\sigma[n_{\rm Na}(t_{\rm out})] = 5.5 \times 10^{-4}$, $\sigma[m_{\rm Na}(t_{\rm out})] = 3.7 \times 10^{-4}$, and $\sigma[w_{\rm Na}(t_{\rm out})] = 3.5 \times 10^{-4}$. These achieved values match the predictions of the photon noise–limited precision.

In order to look for changes in the transit depth in the sodium band relative to the adjacent bands, we calculate, for each of the time series above, the difference in the mean as observed in and out of transit:

$$\Delta n_{\rm Na} = \overline{n_{\rm Na}(t_{\rm in})} - \overline{n_{\rm Na}(t_{\rm out})} = (-23.2 \pm 5.7) \times 10^{-5}$$
$$\Delta m_{\rm Na} = \overline{m_{\rm Na}(t_{\rm in})} - \overline{m_{\rm Na}(t_{\rm out})} = (-13.1 \pm 3.8) \times 10^{-5}$$
$$\Delta w_{\rm Na} = \overline{w_{\rm Na}(t_{\rm in})} - \overline{w_{\rm Na}(t_{\rm out})} = (-3.1 \pm 3.6) \times 10^{-5} . \quad (5)$$

As before, the errors shown are the 1 σ errors of the mean. The results indicate that we have detected a deeper transit in the sodium band for the narrow and medium bandwidths, with a significance of 4.1 σ and 3.4 σ, respectively. We find no significant offset for the wide bandwidth.

Furthermore, we calculate the three quantities in equation (5) for each of the three transits separately. These results confirm the conclusion that there is a deeper signal in the narrow and medium bands. The variations between visits for the same band are not significant, given the precision of the data.

In Figure 3, we plot histograms of the in-transit and out-of-transit data for the narrow band. This plot shows that each of these sets of points is apparently drawn from a normal distribution, with a standard deviation as predicted by photon-counting arguments. However, the in-transit points scatter about a mean that is significantly offset from that defined by the out-of-transit points. This indicates that we have not skewed these distributions by our analysis procedures. Rather, the in-transit observations apparently represent a shifted version of the out-of-transit observations.

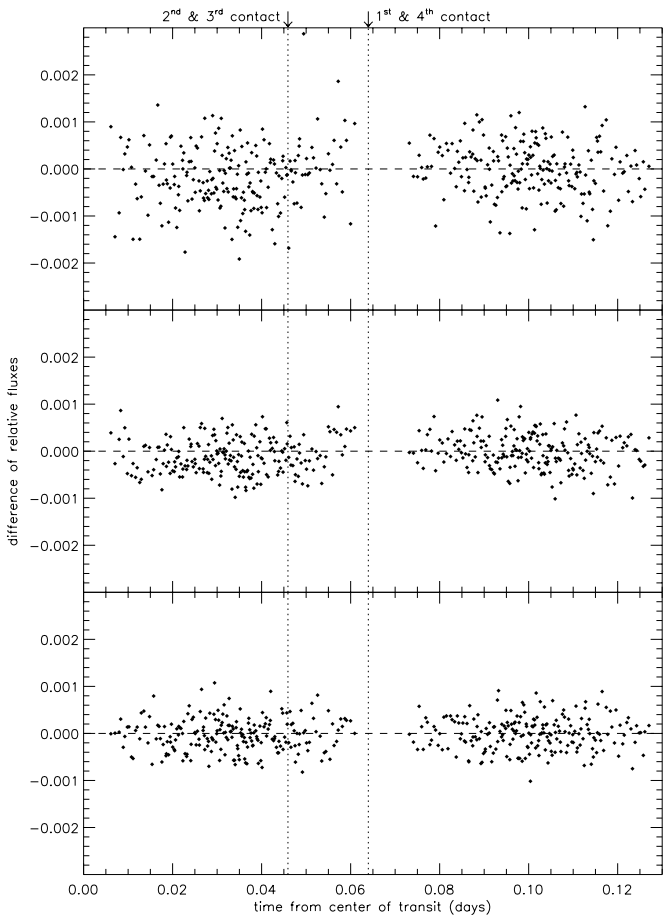


FIG. 2.—Unbinned time series $n_{\rm Na}$ (*top*), $m_{\rm Na}$ (*middle*), and $w_{\rm Na}$ (*bottom*) as a function of absolute time from the center of transit. The means of the in-transit values of $n_{\rm Na}$ and $m_{\rm Na}$ are both significantly offset below 0.

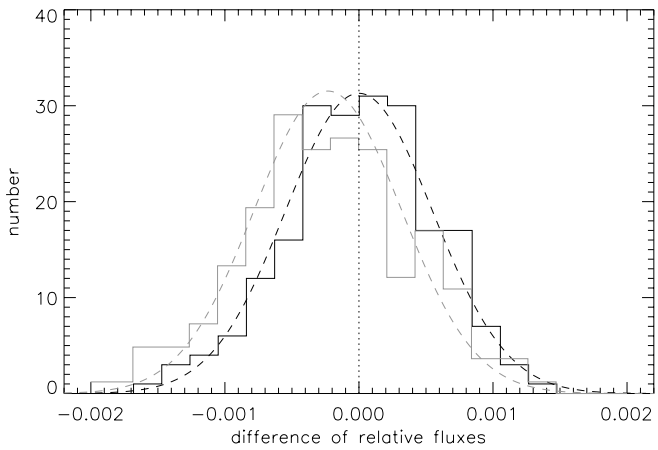


FIG. 3.—*Black solid line*: Histogram of the out-of-transit values of $n_{\rm Na}$ (Fig. 2, *top panel*). *Black dashed curve*: Gaussian distribution, with a mean of 0 and $\sigma = 5.5 \times 10^{-4}$, as prescribed from photon noise predictions, normalized to the same area. *Gray solid line*: Histogram of the in-transit values of $n_{\rm Na}$, renormalized to the same number of observations as the black solid line. *Gray dashed curve*: Gaussian distribution with the same σ as the black curve, but with a mean of -2.32×10^{-4} (the observed value). The gray histogram is significantly offset from 0.

We bin $n_{\rm Na}(t)$ in time and plot these results in Figure 4. These further illustrate that we have observed a deeper transit in the sodium band.

We investigate the possibility that the observed decrement is due to nonlinearity in the STIS CCD. Because the observed value of $\Delta n_{\rm Na}$ is -2.32×10^{-4} for a change in mean intensity from in-transit to out-of-transit of -1.6×10^{-2}, a nonlinearity of $\sim$1% across this range would be required. Gilliland, Goudfrooij, & Kimble (1999) derive an upper limit that is an order of magnitude lower than this. We further test this effect directly by selecting 18 strong stellar absorption features in our observed wavelength range. For each spectral feature, we define a set of bandpasses with the same wavelength range as those listed in Table 1, but now centered on the spectral line. We derive Δn and Δm for each of these as in equation (5). The results are shown in Figure 5. We find no correlation of either Δn or Δm with spectral line depth. These tests also confirm our evaluation of the precision we achieve in equation (5). We find that the values of Δn or Δm are normally distributed, with a mean consistent with 0 and a standard deviation as we found above (eq. [5]).

3. COMPARISON WITH THEORETICAL PREDICTIONS

As described above, the quantity that we observe is the difference between the transit depth in a band centered on the Na D lines and the average of that of two flanking bands, as a function of time from the center of transit. We designated these time series $n_{\rm Na}(t)$, $m_{\rm Na}(t)$, and $w_{\rm Na}(t)$ above. We wish to compare these results with models of the planetary atmosphere. Several steps are required to transform the model predictions into the same quantity as the observable, and we describe these steps here.

We first produce several model calculations of the change in the effective planetary radius as a function of wavelength, as prescribed by Brown (2001). For all the models, we use

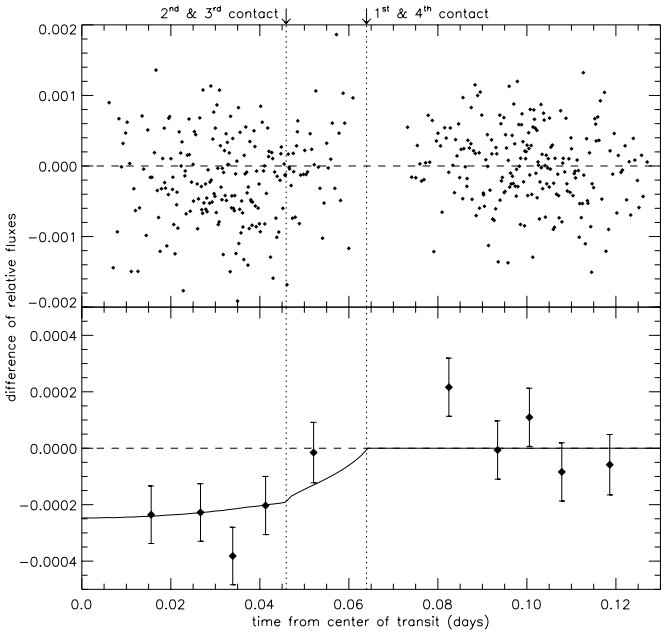


FIG. 4.—*Top*: Unbinned time series $n_{\rm Na}$ (Fig. 2, *top panel*). *Bottom*: These data binned in time (each point is the median value in each bin). There are 10 bins, with roughly equal numbers of observations per bin (42). The error bars indicate the estimated standard deviation of the median. The solid curve is a model for the difference of two transit curves (described in § 3), scaled to the observed offset in the mean during transit, $\Delta n_{\rm Na} = -2.32 \times 10^{-4}$.

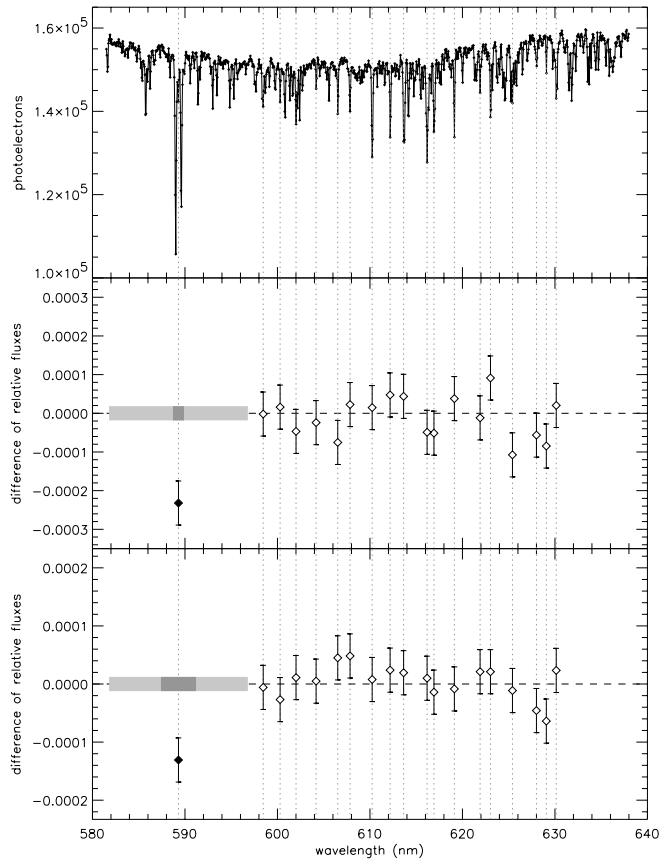


FIG. 5.—*Top*: Typical spectrum of HD 209458, over the full spectroscopic range that we observed. We selected 18 strong features in addition to the Na D lines; these are indicated by vertical dashed lines. *Middle*: Results for the narrow (n) bandpass. The filled diamond is the value of $\Delta n_{\rm Na}$. The wavelength ranges of the bands n_b, n_c, and n_r are shown as horizontal gray bars. We then repeated the analysis, i.e., same bandwidths, but now centered over each of the 18 features indicated. The resulting values are shown as open diamonds. *Bottom*: Corresponding results for the middle (m) bandpass. In each case, the open diamond points are apparently normally distributed, with a mean of 0 and a standard deviation as prescribed by photon statistics. In particular, the residuals do not correlate with the depth of the spectral feature. Some correlations between adjacent points are evident, as expected, because the bandpasses are wider than the separation between points. In the middle and bottom panels, the filled diamond point is inconsistent with a lack of variation at the level of 4.1 σ and 3.4 σ, respectively. Note that the y-axis in the lower panel has been scaled so that the error bars are the same size as those in the middle panel.

the best-fit values from B01 for R_p, R_s, i, a, and M_s, as given in § 2.1. We further specify the planetary mass ($M_p = 0.69$ $M_{\rm Jup}$) and the stellar effective temperature ($T_s = 6000$ K), both as given by Mazeh et al. (2000). We set the equatorial rotational velocity of the planet to $v_{\rm rot} = 2.0$ km s^{-1}. This is the value implied by the measured planetary radius, under the assumption that the planet is tidally locked (i.e., the rotational period is the same as the orbital period). Each model includes the effect of photoionization as described in Brown (2001), which reduces the core strength of the Na D lines, but does not significantly change the wings.

The fiducial model has a cloud deck with cloud tops at a pressure of 0.0368 (0.1/e) bar and solar metallicity (the measured value for HD 209458; Mazeh et al. 2000). We also consider a number of variants to the fiducial model, representing changes to either the metal abundance or the cloud height. These variants are listed in Table 2. For each model (denoted by the index m), we have the theoretical planetary

TABLE 2

MODEL ATMOSPHERE PARAMETERS

Identifier	Cloud Tops (bar)	Metal Abundance (solar)
s1	0.0368	1.00
n1.....	3.68	1.00
n2.....	0.368	1.00
n3.....	0.00368	1.00
n4.....	0.000368	1.00
c1	0.0368	2.00
c2	0.0368	0.50
c3	0.0368	0.01

radius $R_p(\lambda, m)$, where λ denotes the wavelength. For each of these, we renormalize $R_p(\lambda, m)$ so that the average value of the planetary radius over the entire STIS bandpass is the best-fit value determined by B01 (1.347 $R_{\rm Jup}$). These renormalized functions $R_p(\lambda, m)$ are shown in Figure 6.

We use the theoretical model of the stellar surface brightness [$S(\lambda, \mu)$; described in § 2.1] to include the effects of the wavelength-dependent limb darkening of the star. This approach allows us to account for both the continuum limb darkening and the deviations that result in the cores of absorption lines; these can be significant in the case of the sodium features. In general, the limb darkening is less pronounced in the cores of the sodium lines than in the adjacent continuum, and thus, for a planetary radius that is independent of wavelength, the transit light curve near T_c is deeper and more rounded as observed in the continuum than as observed in the core of an absorption line.

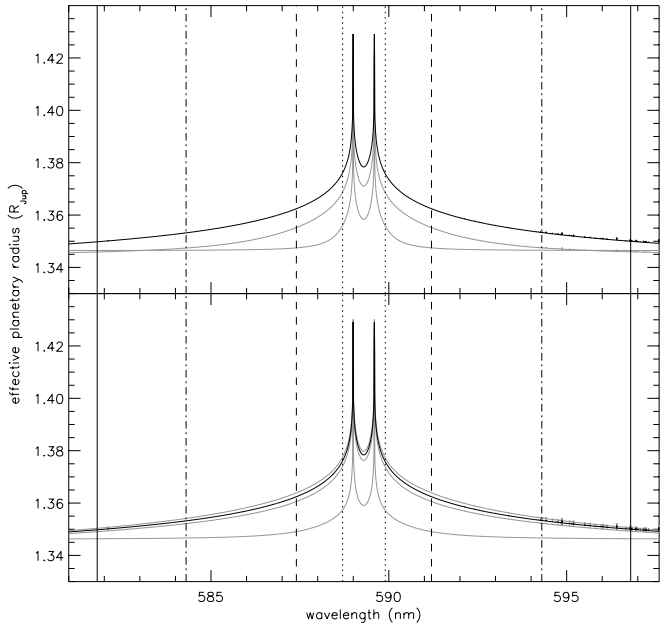


FIG. 6.—Effective planetary radius as a function of wavelength for a variety of atmospheric models. The vertical lines indicate the bandwidths and correspond to those in Fig. 1. In both panels, the black curve shows the planetary radius for the fiducial model (s1). *Top panel*: Variation with cloud height; the upper and lower gray curves are models n3 and n4, respectively. (The results for models n1 and n2 are indistinguishable on this plot from that for s1). *Bottom panel*: Variation with sodium abundance; the gray curves are, from top to bottom, models c1, c2, and c3.

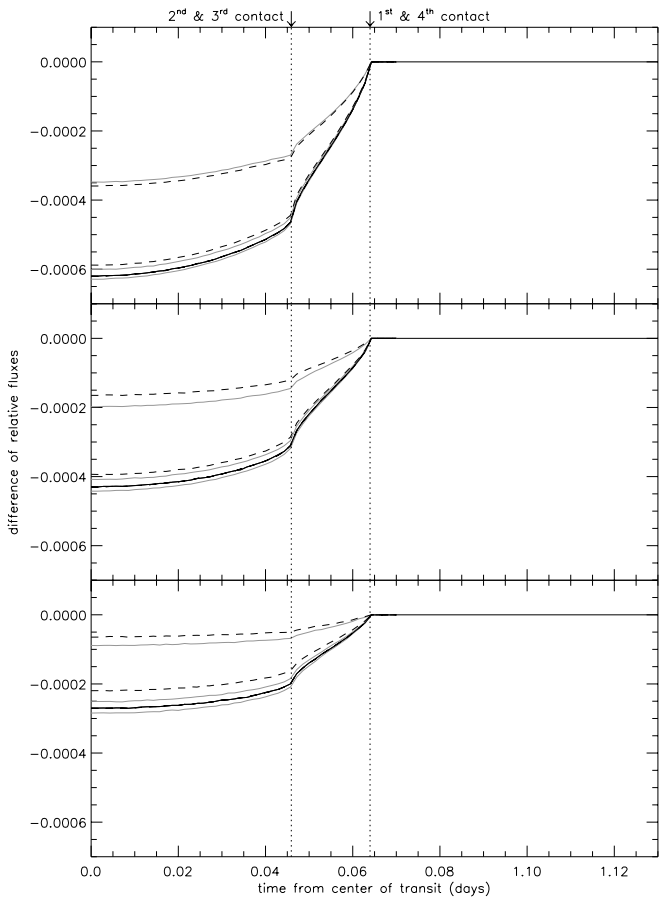


FIG. 7.—*Black solid curve*: Model curve for $n_{\rm Na}$ (*top*), $m_{\rm Na}$ (*middle*), and $w_{\rm Na}$ (*bottom*), for the fiducial model (s1). *Dashed curves*: Variations due to cloud height for models n4 (*upper curve in each panel*) and n3 (*lower curve*). (The results for models n1 and n2 are indistinguishable from that for s1). *Gray solid curves*: Variations due to atomic sodium abundance in models c3, c2, and c1 (*from top to bottom*). These curves may be compared directly with the data presented in Figs. 2 and 4.

We proceed as described in § 2.1, with the exception that $R_p(\lambda, m)$ is now a function of wavelength: for each λ, we produce the theoretical transit curve $T(\lambda, t, m)$. We bin these results in the wavelength bands, as described in § 2, and difference the values in the band centered on the sodium lines from the average of the flanking bands, as prescribed by equation (4). The result is a theoretical time series that closely resembles the observed STIS time series, with the effect of a wavelength-dependent planetary radius included. These model time series are shown in Figure 7 and may be compared directly with the data shown in Figures 2 and 4.

We find that most of the models listed in Table 1 produce differential transits that are significantly deeper than our observational result. Only models n4 and c3, which represent, respectively, extreme high values of cloud height or depleted atomic sodium abundance, produce transits of approximately the correct depth.

4. DISCUSSION

We have detected a significantly deeper transit in the sodium band relative to the adjacent bands. We interpret the signal as due to absorption by sodium in the planetary atmosphere. We are encouraged in this interpretation by the following two considerations. First, a sodium feature in the transmission spectrum of HD 209458 was predicted unanimously by the current modeling efforts (Seager & Sasselov 2000; Brown 2001; Hubbard et al. 2001). Second, observed spectra of L-type objects (see, e.g., Kirkpatrick et al. 1999), T dwarfs (see, e.g., Burgasser et al. 1999), and, in particular, the brown dwarf Gl 229B (see, e.g., Oppenheimer et al. 1998) show very strong absorption from alkali metal lines (Burrows, Marley, & Sharp 2000). These objects span a temperature range of 900–2000 K, which includes the equilibrium temperature of HD 209458b, $T_{\rm eff} = 1430(1 - A)^{1/4}$ K (where A indicates the Bond albedo). (It should be noted that these objects are at roughly the same temperature as HD 209458b for very different reasons: the planet is heated by its proximity to the parent star, whereas the temperatures for the other objects are set by their ongoing contraction.)

In the following discussion, we first consider alternate interpretations of our result, then discuss the constraints that we can place on the planetary atmosphere, and finish by looking ahead to near-future complementary observations.

4.1. *Alternate Explanations*

We must take care that the observed decrement is not the result of the distinctive limb darkening exhibited by the sodium line relative to that of the adjacent continuum. In order to quantify the amplitude of this effect, we generated model transit curves (for a planet of *constant* radius), as described in § 2.1, and integrated these in λ over the nine bandpasses listed in Table 1. We then re-created the linear combination of these results as given in equation (4). We found that the predicted offsets were:

$$\begin{aligned}
\Delta n_{\rm Na}({\rm theory; constant}\ R_p) &= +1.52 \times 10^{-5} \\
\Delta m_{\rm Na}({\rm theory; constant}\ R_p) &= +0.39 \times 10^{-5} \\
\Delta w_{\rm Na}({\rm theory; constant}\ R_p) &= +0.47 \times 10^{-5}\ . \qquad (6)
\end{aligned}$$

These values are much smaller than the signal we detect. Moreover, they are of the opposite sign: because the net decrement toward the limb is less in the sodium line than in the adjacent continuum, the transit as observed in a band centered on the sodium lines would be expected to be *less* deep near T_c than that observed in a band in the adjacent spectral region. We note that the above quantities should be subtracted from the observed values of $\Delta n_{\rm Na}$, $\Delta m_{\rm Na}$, and $\Delta w_{\rm Na}$ given in equation (5) for comparison with future modeling efforts that do not explicitly include the wavelength-dependent limb darkening. For the purposes of the present paper, our models explicitly account for this effect by making use of the model stellar surface brightness, and thus no adjustment is needed.

A second concern is that the star might appear *smaller* when observed at the wavelength of the sodium lines, producing a deeper transit for the same-sized planet. In fact, we expect the opposite to be true: the solar limb should be slightly *larger* in the core of the Na D lines because of the great opacity in these lines. Model calculations (E. H. Avrett 2001, private communication) yield an intensity-weighted solar radius increase, after averaging over even the narrowest bandpass containing the Na D lines, of less than 10 km. This will have a completely negligible effect on the observed transit depth in the bandpass containing the Na D lines.

4.2. *Constraints on the Planetary Atmosphere*

Our fiducial model (s1), which has cloud tops at 0.04 bar and a solar abundance of sodium in atomic form, predicts values for $\Delta n_{\rm Na}$ and $\Delta m_{\rm Na}$ that are $\sim$3 times deeper than we observe. This conclusion awaits confirmation from other, more detailed models, such as those constructed by Seager & Sasselov (2000) and Hubbard et al. (2001). Here we consider several possible physical effects that may contribute to the reduced sodium absorption relative to the predictions of our model.

It may be that a significant fraction of atomic sodium has combined into molecules, which may be either present as gaseous species, or sequestered from the atmosphere as condensates. Chemical equilibrium models for substellar and planetary atmospheres (Fegley & Lodders 1994, 1996; Burrows & Sharp 1999; Lodders 1999) indicate that Na_2S, NaCl, NaOH, NaH, and more complicated species (such as $NaAlSi_3O_8$) may be present in the planetary atmosphere. In particular, Lodders (1999) finds that, at these temperatures, the competition for sodium is predominantly between Na_2S (*solid*) and monatomic Na (*gas*). At temperatures above the Na_2S condensation line, sodium is predominantly in atomic form, and gases such as NaCl, NaOH, and NaH never become the most abundant sodium-bearing species (K. Lodders 2001, private communication). If the disparity between the observed values for $\Delta n_{\rm Na}$ and $\Delta m_{\rm Na}$ and the predictions for these quantities based on our fiducial model (s1) is due entirely to this effect (and is not, for example, mitigated by the effect of high cloud decks), then this would indicate that less than 1% of the sodium is present in atomic form. This statement is based on the fact that even our model c3 fails to reproduce the observed values.

Our current models (Brown 2001) account for the ionization of sodium by the large stellar flux incident upon the planetary atmosphere. However, it is possible that the effect is larger than predicted by our calculations. This would require a sink for free electrons, the effect of which would be to lower the recombination rate.

Perhaps HD 209458 began with a depleted sodium abundance, or, more generally, a depleted metal abundance. The current picture of gas giant planet formation predicts that planets should present a metallicity at or above the value observed in the parent star; Jupiter and Saturn are certainly metal-rich relative to the Sun (see discussion in Fegley & Lodders 1994). Metallicity apparently plays an important role in the formation of planets: parent stars of close-in planets are typically metal-rich (Gonzalez 1997, 2000) relative to their counterparts in the local solar neighborhood (Queloz et al. 2000b; Butler et al. 2000). Furthermore, the observed lack of close-in giant planets in the globular cluster 47 Tuc (Gilliland et al. 2000) may be due, in part, to a reduced planet formation rate caused by the low metallicity of the globular cluster. The relationship linking metallicity and planet formation is not clear.

Clouds provide a natural means of reducing the sodium absorption, by creating a hard edge to the atmosphere and thereby reducing the effective area of the atmosphere viewed in transmission. If the difference between the observed values of $\Delta n_{\rm Na}$ and $\Delta m_{\rm Na}$ and the predictions for these quantities based on our fiducial model (s1) is due entirely to clouds, then this would require a very high cloud deck, with cloud tops above 0.4 mbar (model n4). Ackerman & Marley (2001) have recently produced algorithms to model cloud formation in the atmospheres of extrasolar planets. The effect of the stellar UV flux on the atmospheric chemistry has not been explicitly included. We urge investigations of the production of condensates, such as photochemical hazes, by this mechanism. Such photochemical hazes are present in the atmospheres of the gas giants of the solar system and produce large effects upon the observed reflectance spectra of these bodies (Karkoschka 1994). The stellar flux incident upon the atmosphere of HD 209458b is roughly 20,000 times greater than that upon Jupiter.

4.3. *Future Observations*

In the present work, we have demonstrated that, by using existing instruments, it is possible to begin the investigation of the atmospheres of planets orbiting other stars. Wide-field surveys conducted by dedicated small telescopes (see, e.g., Borucki et al. 2001; Brown & Charbonneau 2000)[7] promise to detect numerous close-in, transiting planets over the next few years. The parent stars of these planets should be sufficiently bright to permit similar studies of the planetary atmosphere.

Based on the results presented here, we believe that the observed value of sodium absorption from the planetary atmosphere may have resulted from a high cloud deck, a low atomic sodium abundance, or a combination of both. Observations of the transmission spectrum over a broader wavelength range should allow us to distinguish between these two broad categories of models (Fig. 8). If the effect is predominantly due to clouds, the transmission spectrum from 300 to 1000 nm will show little variation with wavelength, other than additional alkali metal lines. If, on the other hand, the clouds are very deep or not present, then the transmission spectrum may show deep features redward of 500 nm due to water and absorption due to Rayleigh scattering blueward of 500 nm. These are only two extremes of the many possibilities; the actual case may share characteristics of both of these effects. Further diagnostics could be provided by near-IR spectroscopy, which could detect

[7] See also http://www.hao.ucar.edu/public/research/stare/stare.html, maintained by T. Brown and D. Kolinski.

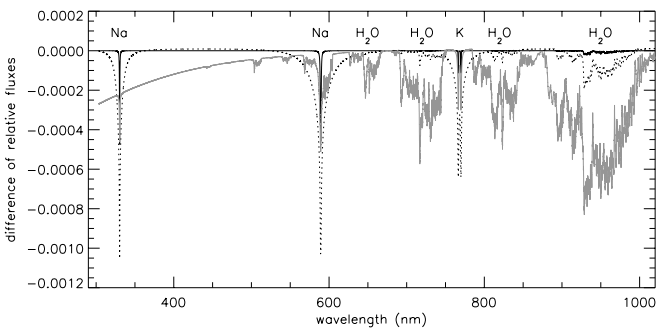


FIG. 8.—Three model transmission spectra for HD 209458, over a wavelength range that exceeds that of our current data set. The fiducial model (s1), with a solar abundance of sodium and cloud tops at 0.0368 bar, is shown as a dotted line. This model is excluded by the data, which do not permit such a deep sodium feature. One possibility is that very high clouds reduce the depth of the sodium absorption feature; such a model is shown as the black solid line. Another possibility is that the abundance of atomic sodium in the planetary atmosphere is reduced greatly from the solar value; this is shown as the gray solid line. Observations of the transmission spectrum over the range shown here should allow for us to distinguish between these two broad categories of models.

features due to molecular species (such as H_2O, CO, and CH_4) that are expected to be present in planetary transmission spectra (Seager & Sasselov 2000; Brown 2001; Hubbard et al. 2001). Suitable observations in the 1–5 μm region would allow inferences about the atmosphere's thermal structure and composition, permitting a more definite interpretation of the sodium signature. Brown et al. (2000) have presented preliminary near-IR spectra of HD 209458 in and out of transit. These spectra demonstrate that it should be possible to search for near-IR atmospheric signatures with existing instruments, such as the NIRSPEC spectrograph (McLean et al. 1998) on the Keck II Telescope.

Observations of the reflected-light spectrum (wavelength-dependent geometric albedo), as pursued for the τ Boo system (Charbonneau et al. 1999; Collier Cameron et al. 1999), would complement the results of transmission spectroscopy. Predictions for the albedo as a function of wavelength vary by several orders of magnitude (Seager & Sasselov 1998; Marley et al. 1999; Goukenleuque et al. 2000; Sudarsky, Burrows, & Pinto 2000). These observations should be facilitated in the case of a transiting system (Charbonneau & Noyes 2000). If possible, the observation of the phase function (variation in the reflected light with orbital phase) would constrain greatly the nature of particulates in the planetary atmosphere (Seager, Whitney, & Sasselov 2000). Observations of molecular absorption features from thermal emission spectra, such as sought in the recent study of the τ Boo system (Wiedemann, Deming, & Bjoraker 2001), would clearly complement these studies. Finally, infrared photometry of the secondary eclipse would provide a direct measurement of the effective temperature of the planetary atmosphere, should the requisite precision be achieved.

We thank Steven Beckwith for the grant of Director's Discretionary Time for this project. We are grateful to the *HST* STIS and operations teams, especially Helen Hart, Gerard Kriss, and Jeff Valenti for their prompt and insightful help in resolving the database error experienced during the first transit. We thank the referee, William Hubbard, for his comments, as well as for his prompt review of the manuscript. We also thank the many theorists, including Travis Barman, Adam Burrows, Katharina Lodders, Mark Marley, Dimitar Sasselov, and Sara Seager, for their thoughts on the constraints that could be placed on the planetary atmosphere. Support for proposals HST-GO-08789.01-A and HST-GO-08789.02-A was provided by NASA through a grant from the Space Telescope Science Institute, which is operated by the Association of Universities for Research in Astronomy, Inc., under NASA contract NAS 5-26555. Further support for this work was provided through NASA grant NAG 5-10854.

REFERENCES

Ackerman, A. S., & Marley, M. S. 2001, ApJ, 556, 872
Borucki, W. J., Caldwell, D., Koch, D. G., Webster, L. D., Jenkins, J. M., Ninkov, Z., & Showen, R. 2001, PASP, 113, 439
Brown, T. M. 2001, ApJ, 553, 1006
Brown, T. M., & Charbonneau, D. 2000, in ASP Conf. Ser. 219, Disks, Planetesimals, and Planets, ed. F. Garzón, C. Eiroa, D. de Winter, & T. J. Mahoney (San Francisco: ASP), 557
Brown, T. M., Charbonneau, D., Gilliland, R. L., Noyes, R. W., & Burrows, A. 2001, ApJ, 552, 699 (B01)
Brown, T. M., et al. 2000, AAS, 197, 11.05
Bundy, K. A., & Marcy, G. W. 2000, PASP, 112, 1421
Burgasser, A. J., et al. 1999, ApJ, 522, L65
Burrows, A., Marley, M. S., & Sharp, C. M. 2000, ApJ, 531, 438
Burrows, A., & Sharp, C. M. 1999, ApJ, 512, 843
Butler, R. P., Vogt, S. S., Marcy, G. W., Fischer, D. A., Henry, G. W., & Apps, K. 2000, ApJ, 545, 504
Charbonneau, D., Brown, T. M., Latham, D. W., & Mayor, M. 2000, ApJ, 529, L45
Charbonneau, D., & Noyes, R. W. 2000, in ASP Conf. Ser. 219, Disks, Planetesimals, and Planets, ed. F. Garzón, C. Eiroa, D. de Winter, & T. J. Mahoney (San Francisco: ASP), 461
Charbonneau, D., Noyes, R. W., Korzennik, S. G., Nisenson, P., Jha, S., Vogt, S. S., & Kibrick, R. I. 1999, ApJ, 522, L145
Collier Cameron, A., Horne, K., Penny, A., & James, D. 1999, Nature, 402, 751
Coustenis, A., et al. 1998, ASP Conf. Ser. 134, Brown Dwarfs and Extrasolar Planets, ed. R. Rebolo, E. L. Martín, & M. R. Zapatero Osorio (San Francisco: ASP), 296
Cox, A. N., ed. 2000, Allen's Astrophysical Quantities (4th ed.; New York: AIP Press)
Deeg, H. J., Garrido, R., & Claret, A. 2001, NewA, 6, 51
Fegley, B., Jr., & Lodders, K. 1994, Icarus, 110, 117
———. 1996, ApJ, 472, L37
Gilliland, R. L., Goudfrooij, P., & Kimble, R. A. 1999, PASP, 111, 1009
Gilliland, R. L., et al. 2000, ApJ, 545, L47
Gonzalez, G. 1997, MNRAS, 285, 403
Gonzalez, G. 2000, in ASP Conf. Ser. 219, Disks, Planetesimals, and Planets, ed. F. Garzón, C. Eiroa, D. de Winter, & T. J. Mahoney (San Francisco: ASP), 523
Goukenleuque, C., Bézard, B., Joguet, B., Lellouch, E., & Freedman, R. 2000, Icarus, 143, 308
Henry, G. W., Marcy, G. W., Butler, R. P., & Vogt, S. S. 2000, ApJ, 529, L41
Hubbard, W. B., Fortney, J. J., Lunine, J. I., Burrows, A., Sudarsky, D., & Pinto, P. 2001, ApJ, 560, 413
Jha, S., Charbonneau, D., Garnavich, P. M., Sullivan, D. J., Sullivan, T., Brown, T. M., & Tonry, J. L. 2000, ApJ, 540, L45
Karkoschka, E. 1994, Icarus, 111, 174
Kirkpatrick, J. D., et al. 1999, ApJ, 519, 802
Lodders, K. 1999, ApJ, 519, 793
Marley, M. S., Gelino, C., Stephens, D., Lunine, J. I., & Freedman, R. 1999, ApJ, 513, 879
Mazeh, T., et al. 2000, ApJ, 532, L55
McLean, I. S., et al. 1998, Proc. SPIE, 3354, 566
Moutou, C., Coustenis, A., Schneider, J., St. Gilles, R., Mayor, M., Queloz, D., & Kaufer, A. 2001, A&A, 371, 260
Oppenheimer, B. R., Kulkarni, S. R., Matthews, K., & van Kerkwijk, M. H. 1998, ApJ, 502, 932
Queloz, D., Eggenberger, A., Mayor, M., Perrier, C., Beuzit, J. L., Naef, D., Sivan, J. P., & Udry, S. 2000a, A&A, 359, L13
Queloz, D., et al. 2000b, A&A, 354, 99
Rauer, H., Bockelée-Morvan, D., Coustenis, A., Guillot, T., & Schneider, J. 2000, A&A, 355, 573
Sackett, P. D. 1999, in Planets Outside the Solar System: Theory and Observations, ed. J.-M. Mariotti & D. Alloin (NATO ASI Ser. C, 532; Dordrecht: Kluwer), 189
Seager, S., & Sasselov, D. D. 1998, ApJ, 502, L157
———. 2000, ApJ, 537, 916
Seager, S., Whitney, B. A., & Sasselov, D. D. 2000, ApJ, 540, 504
Sudarsky, D., Burrows, A., & Pinto, P. 2000, ApJ, 538, 885
Wiedemann, G., Deming, D., & Bjoraker, G. 2001, ApJ, 546, 1068